Buckling of a rod penetrating into granular media

A. Seguin and P. Gondret

Laboratoire FAST, Univ. Paris-Sud, CNRS, Université Paris-Saclay, F-91405, Orsay, France

We investigate experimentally the possible buckling of a thin rod when penetrating downwards into a granular packing. When its bottom end reaches a specific depth, the rod may start buckling provided that the embrace is not enough to stop that phenomenon. The critical rod depth z_c at buckling is observed to scale with the rod length L either as $1/L$ or $1/L^2$. These two scalings are shown to arise from the two resistant force terms that come into play during the rod penetration: a pressure force at the bottom of the rod that increases linearly with depth and a frictional force on the rod side that increases quadratically with depth. At the buckling point, the destabilizing force corresponds to the expected value given from conventional Euler's critical load for a rod bottom end considered as fixed in the granular clutch. Finally, we draw a buckling-nonbuckling phase diagram in a parameter space given by the rod aspect ratio and a rod-to-grain stress ratio.

I. INTRODUCTION

The complex physics of granular matter has been addressed in numerous studies in recent years with some important progress in the modeling of its puzzling rheology, even if its liquid-solid transition remains still unclear [1]. In this context, the motion of objects into granular matter has received much attention with some geological or biological interest like impact cratering [2] on planets and asteroids or animal locomotion on or through sand [3]. In most studies, these objects are of different shapes such as spheres [4,5] or cylinders [6–12], disks or plates [13], or even more complex shape [14], but nondeformable. As in hydrodynamics, both drag and lift forces have been measured [11,15]. In most cases, these forces do not depend significantly on velocity [6,9,10,16] but increase with depth [9–13]. Depending on the shape of objects, the force variation with depth may be linear or not [17–19]. More recently, some possible deformation of objects moving into granular matter have been considered for addressing the problem of the root growth in soil [20]. A thin lamella fully embedded in a two-dimensional and horizontal disk assembly is pushed at one end, whereas the other end is free and the deformation is observed and analyzed in terms of flexion [21]. Numerical simulations with discrete element methods have been also recently developed to mimic root growth and deformation within a granular assembly [22].

In this paper, we look at the possible buckling of a thin rod when pushed downward into a granular bed. As the vertical drag force exerted by the grains on the rod increases with depth the critical force for buckling may be reached, but as the radial stress also increases with depth [23] the rod may not buckle. Rod buckling should be governed thus by the complex interplay between the destabilizing increasing resistive force with depth and the increasing stabilizing lateral pressure forces. Contrary to conventional buckling where the destabilizing force is at the rod tips only, the friction force acting on the lateral surface of the "granular immersed" rod is shown to exist in addition to the resulting pressure force at the bottom of the rod. As these two force terms do not have the same depth scaling,

we show that the critical depth at buckling is given by two different scalings depending on whether one force term or the other dominates. Finally, we draw a phase diagram for the rod buckling or nonbuckling and show that the buckling condition is given by one main criterion.

II. EXPERIMENTAL SETUP

The experiment consists in plunging downwards at a constant velocity a vertical thin rod into granular matter. We use rods of different length L in the range $300 \leqslant L \leqslant 1100$ mm and different diameter D in the range $2 \leqslant D \leqslant 6$ mm. The rods are very thin with a very large length-to-diameter ratio $50 \leqslant L/D \leqslant 550$ and are made of materials with different elastic Young modulus in the range $3 \lesssim E \lesssim 130$ GPa: PMMA or PVC ($E \simeq 3$ GPa), wood ($E \simeq 10$ GPa), aluminum ($E \simeq 58$ GPa), and copper ($E \simeq 130$ GPa). Granular matter consists in sieved glass beads of diameter in the range $0.3 \leqslant d \leqslant 5$ mm and density $\rho = 2.5 \times 10^3$ kg/m^3. The beads are rather monodisperse with a relative size dispersion smaller than 10%. The granular medium is prepared by pouring into a cylindrical container of inner diameter Δ and of height H a volume of beads larger than the volume of the container before tapping the container a few times and then leveling the grains off the cylinder with a straight ruler. Following this procedure, we obtain a well reproducible dense packing fraction $\phi \simeq 0.63$ with only small variations. The container was chosen large enough to avoid any possible wall effect. In particular, the container-to-rod diameter ratio is in the range $13 < \Delta/D < 40$, which is high enough for glass beads to avoid any sidewall effects [24,25]. The container was chosen also deep enough to avoid any bottom wall effect [24] with $40 < H/D < 400$. In most of the experiments presented here, $\Delta = 80$ mm and $H = 250$ mm or more (up to 800 mm). The rod is clamped vertically at its top end to a moving translation guide, whereas its down end is let free, initially just above the horizontal granular surface. The vertical rod is then moved down at an imposed velocity in the range $1 < V < 10^2$ mm/s along
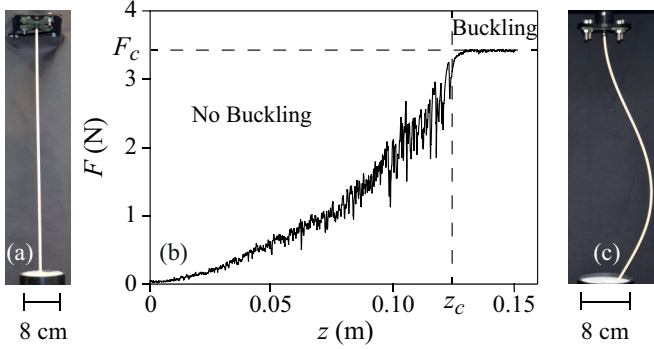
FIG. 1. (a)–(c) Images of the rod when penetrating into a granular packing (a) before and (c) after its buckling. (b) Experimental penetration force F as a function of the penetration depth z for a thin PVC rod of diameter $D = 4$ mm and length $L = 600$ mm into glass beads of diameter $d = 1$ mm. The rod buckling arises at $z_c = 0.13$ m for $F_c = 3.4$ N.

the vertical axis of the cylindrical container and penetrates thus gradually into the granular packing. Images of the rod are taken from the side. The rod remains first straight [see Fig. 1(a)] but then may buckle [see Fig. 1(c)] at a given critical penetration depth z_c. For a given set of experimental conditions, we made ten different runs to measure the mean value and the standard deviation of z_c. With a force sensor at the tip of the rod, one can also measure at a high resolution ($\simeq 10$ mN) the instantaneous vertical force exerted by the grains on the penetrating rod provided that $L < 1$ m for geometrical constraints. The evolution of the measured force as a function of the penetration depth z of a PVC rod of length $L = 600$ mm and diameter $D = 4$ mm in a packing of $d = 1$ mm glass beads is shown in Fig. 1(b). The typical curve of Fig. 1(b) corresponds to the ensemble average over ten runs. Despite large force fluctuations inherent of granular matter [6,14], a gradual force increase is observed with the penetration depth z up to a critical depth value $z_c \simeq 130$ mm, where the force then saturates at the critical value $F_c \simeq 3.4$ N. At this critical point, rod buckling occurs suddenly. In all the experiments we take care that the critical depth value at buckling is far enough from the bottom wall with always the condition $H - z_c > 10D$ verified.

III. EXPERIMENTAL RESULTS

The first important result is that these observations do not depend on the penetration velocity. Indeed, the critical depth for buckling z_c shown in Fig. 2(a) for a PVC rod of diameter $D = 4$ mm and length $L = 1000$ mm into $d = 1$ mm glass beads is roughly constant within the present range of velocity from about one mm/s to a few cm/s. This is not surprising as the drag force for moving objects in grains is known to not depend significantly on velocity in most experiments where the velocity is high enough for not being sensitive to any possible vibrations and low enough for not being in the inertial regime [16]. By contrast, the critical depth z_c for buckling depends strongly on the rod geometrical and mechanical characteristics. As shown in Fig. 2(b), z_c decreases for increasing L whatever the rod diameter and material. The three curves of Fig. 2(b)
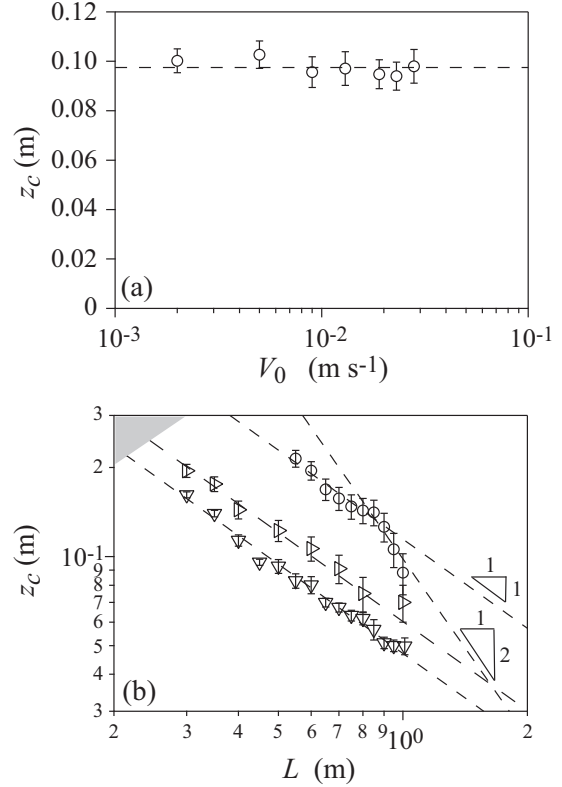

FIG. 2. (a) Penetration depth z_c at buckling as a function of the penetration velocity V. ($\circ$) Data for a PVC rod of diameter $D = 4$ mm and length $L = 1000$ mm into glass beads of diameter $d = 1$ mm and (- - -) line of constant $z_c = 97$ mm. (b) Penetration depth z_c as a function of the rod length L at $V = 20$ mm/s for ($\circ$) a $D = 4$ mm PVC rod, ($\triangledown$) a $D = 3$ mm PMMA rod, and ($\triangleright$) a $D = 3$ mm wood rod. (- - -) Power law fits $z_c = A/L$ and $z_c = B/L^2$ of the data with (o) $A = 0.14 \pm 0.01$ m^2 and $B = 0.09 \pm 0.01$ m^3 and ($\triangledown$) $A = 0.047 \pm 0.001$ m^2 and ($\triangleright$) $A = 0.060 \pm 0.001$ m^2. The shaded region corresponding to $z_c > L$ is not allowed.

corresponding to rods of two different diameters ($D = 3$ and 4 mm) and of two different elastic modulus ($E = 3$ and 10 GPa) show also that z_c is smaller for thicker and stiffer rods. Looking carefully to the curve obtained for a $D = 4$ mm PVC rod (circle symbols), it appears that the decrease of z_c with L shows two different regimes: a first decrease with the scaling $z_c \sim L^{-1}$ for $L \lesssim 0.9$ m followed by another decrease with a scaling close to $z_c \sim L^{-2}$ for $L \gtrsim 0.9$. This second scaling is not observed for the two other data sets.

Let us now look at the critical force F_c at buckling as a function of the rod length L. The results reported in Fig. 3(a) for the $D = 4$ mm PVC rod show that F_c decreases for increasing L with the scaling $F_c \sim L^{-2}$. Such a scaling is expected from a classical buckling criterion. Indeed, the critical buckling force for a free rod is

$$F_{c0} = \left(\frac{\pi}{4}\right)^3 \frac{E D^4}{(\varepsilon L)^2}, \qquad (1)$$

where ε is a parameter depending on the boundary conditions for the two rod ends: e.g., $\varepsilon = 1/2$ for two fixed boundaries or $\varepsilon \simeq 0.7$ for one fixed boundary and the other with a pinned boundary. Figure 3(b) shows the value of ε that can be deduced
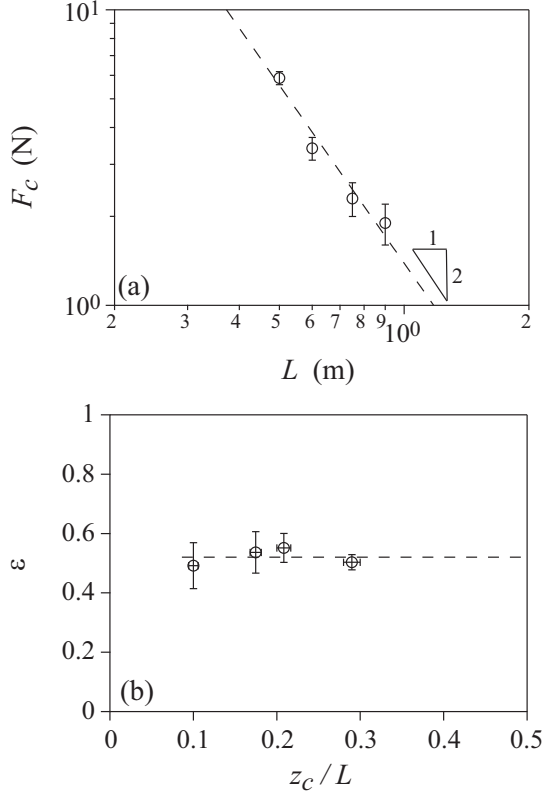
FIG. 3. (a) Critical buckling force F_c as a function of the rod length L for a $D = 4$ mm PVC rod into $d = 1$ mm glass beads. (- - -) Power law fit $F_c = A/L^2$ with $A = 1.5 \pm 0.1$ N m^2. (b) Boundary condition parameter ϵ as a function of the relative penetration depth at buckling z_c/L for the same data set. (- - -) Line of constant $\epsilon = 0.52$.

from each data point of Fig. 3(a). We see that ε is about constant with the value $\varepsilon = 0.52 \pm 0.04$ very close to the 1/2 value corresponding to a fixed boundary at each rod end. A fixed boundary condition is clearly imposed at the top end by the present experimental setup, but a fixed condition seems to be also imposed at the bottom end by the granular radial confinement in the range of the present experiments, where $z_c/L \gtrsim 0.1$ and $z_c/D \gtrsim 20$. In such a case, the depth penetration is high enough for the rod to be embraced in the granular packing. This about constant value of ε observed in Fig. 3(b) explains the simple scaling $F_c \sim L^{-2}$ observed in Fig. 3(a). Note that no simple scaling appears either for the critical depth penetration or for the critical force at buckling as a function of the free length of the rod $L - z_c$. In the following, we thus consider the total rod length L with two fixed boundary conditions at each end in the modeling.

IV. MODELING

Let us now consider a simple modeling for the upwards vertical drag force exerted by the granular medium on the rod. The granular "pressure" p that exists in granular matter may be considered as increasing linearly with depth as the hydrostatic pressure in classical fluids and may thus be written as $p = \phi\rho g z$, where $\phi\rho$ is the effective density of the granular packing.

The total force is expected to come from two parts: (i) the granular force pressure at the bottom tip of the rod of circular cross section $\pi D^2/4$ and (ii) the granular frictional force on the lateral side of the "granular immersed" rod part of area $\pi D z$ with the grain-rod friction coefficient μ. The resultant upward vertical force is thus expected to have the following form:

$$F = \frac{\pi C_1}{4}\phi\rho g D^2 z + \frac{\pi C_2}{2}K\mu\phi\rho g D z^2, \qquad (2)$$

where C_1 and C_2 are numerical prefactors and K is the coefficient of redirection of the normal stress components σ_{ii} from the vertical z direction to the radial r direction ($p = \sigma_{zz} = \sigma_{rr}/K$). The corresponding resulting force when made nondimensionless by the weight of a volume $\pi D^3/4$ of grains corresponding to a rod penetration depth $z = D$ is

$$\frac{F}{\pi\phi\rho g D^3/4} = C_1\frac{z}{D} + 2C_2 K\mu\left(\frac{z}{D}\right)^2. \qquad (3)$$

The first term in the right-hand side of Eq. (3) should dominate at low penetration depth ($z/D \ll 1$), whereas the second force term should dominate at large penetration depth ($z/D \gg 1$), so that the force should approach a linear scaling $F \sim z$ for $z/D \ll 1$ but a quadratic scaling $F \sim z^2$ for $z/D \gg 1$. The crossover between the two expected regimes where the two terms balance should occur for $z/D = C_1/2C_2 K\mu$. The $F(z)$ measurements of Fig. 1 are now shown in dimensionless form in the log-log plot of Fig. 4(a). The experimental data before buckling are well fitted by Eqs. (2) and (3) with $C_1 \simeq 17$ and $C_2 K\mu \simeq 0.85$, with a crossover between the successive linear and quadratic regimes at $z/D = C_1/2C_2 K\mu \simeq 10$ depending on the C_1 and $C_2 K\mu$ values.

In our experiments corresponding to the vertical penetration of thin rods ($L/D \gg 1$) we see a linear regime in the experimental range $10^0 \lesssim z/D \lesssim 10^1$ followed by a supralinear (quadratic regime) in the experimental range $10^1 \lesssim z/D \lesssim 10^2$. Note that in the recent experiments of [25] corresponding to the vertical penetration of very thick "rods" ($L/D \sim 1$) a first sublinear regime at very low penetration depth is observed, in the range $10^{-2} \lesssim z/d \lesssim 10^{-1}$, followed by a linear regime at larger depth, in the range $10^{-1} \lesssim z/d \lesssim 10^0$. The first sublinear regime, which corresponds to the transient growing of a conical static zone of grains at the bottom tip of the rod [25], is too small to be observed in the present experiments with very thin rods.

The two force terms of Eqs. (2) and (3) with the two different depth scalings $F \sim z$ and $F \sim z^2$ explain the different observed scalings for the penetration depth at buckling as a function of the rod length observed in Fig. 2(b). Indeed, when the linear force term dominates, the penetration depth at buckling should be given from the buckling criterion of Eq. (1) by $z_c/D \simeq (\pi^2/16\varepsilon^2\phi C_1)(ED/\rho g L^2)$, whereas $z_c/D \simeq (\pi^2/32\varepsilon^2\phi C_2 K\mu)^{1/2}(ED/\rho g L^2)^{1/2}$ when the quadratic force term dominates. The scaling $z_c \sim L^{-1}$ is observed for the three rods shown in Fig. 2(b), whereas the scaling $z_c \sim L^{-2}$ is only observed for the rod that is thick enough (large enough D) but soft enough (low enough E). The buckling onset for all the data sets is reported in Fig. 4(b), where the dimensionless critical penetration depth z_c/D is shown as a function of the stiffness parameter $ED/\rho g L^2$. In this plot, all the data for different materials (different E) and rod

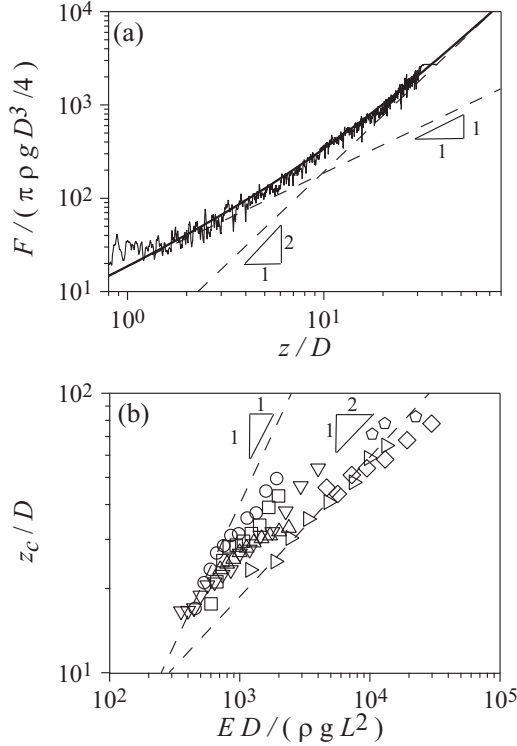FIG. 4. (a) Dimensionless vertical force $\tilde{F} = 4F/\pi\phi\rho gD^3$ on the rod as a function of the dimensionless rod penetration z/D. Same experimental data as in Fig. 1 together with (——) the best fit by Eq. (3) with $C_1 = 17$ and $C_2K\mu = 0.85$ and (- - -) the two expected asymptotic scalings $\tilde{F} \sim z/D$ and $\tilde{F} \sim (z/D)^2$ at small and large z/D, respectively. (b) Dimensionless rod penetration at buckling z_c/D as a function of the stiffness parameter $ED/\rho gL^2$ for rods of different elastic modulus E and diameter D into $d = 1$ mm glass beads: (o) $D = 4$ mm in PVC, ($\triangledown$) $D = 3$ mm in PMMA, ($\triangleright$) $D = 3$ mm in wood, ($\diamond$) $D = 2$ mm in aluminum, ($\square$) $D = 5$ mm in PVC, ($\triangle$) $D = 6$ mm in PMMA, and ($\hexagon$) $D = 2$ mm in copper.

diameter D gathered close to one master curve with, however, a large dispersion arising from large dispersion in the values of C_1 and $C_2K\mu$ due to different rod-grain interactions. The corresponding values of C_1 and $C_2K\mu$ are displayed in Fig. 5 as a function of the rod-to-grain size ratio D/d. The C_1 values are rather dispersed around the mean value $C_1 \simeq 30 \pm 15$ with no clear variation with D/d. In the case of very large rod-to-grain size ratio ($D/d \gg 1$), where the granular packing acts as a continuum medium on the rod, Ref. [25] shows that C_1 depends nonlinearly on the internal friction coefficient of the granular packing due to curved stress lines originating from a steady conical static zone at the bottom of the rod and developing through the Mohr-Coulomb slip criterion [18]. The C_1 values found by [25] for large rod-to-grain size ratio ($D/d > 10$) are between 14 and 32 for glass beads of internal friction angles ranging from $22°$ to $28°$. Our measurements with the smallest glass beads $d = 0.3$ mm (green symbols in Fig. 5) for which $D/d > 10$ correspond to $C_1 \simeq 26$, which is in the expected range. Our measurements with larger grains are more dispersed which is expected from the corresponding low values of rod-to-grain size ratio ($D/d < 10$). The $C_2K\mu$ values shown in Fig. 5(b) display also large error bars but seem
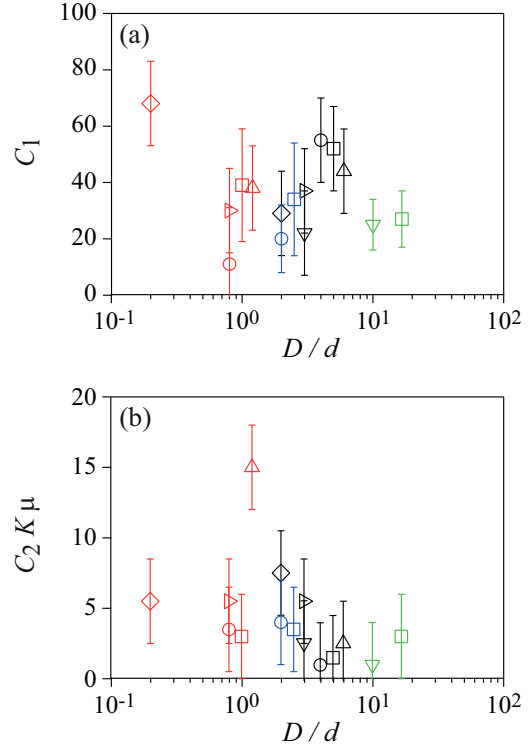

FIG. 5. Coefficients (a) C_1 and (b) $C_2K\mu$ of the two force terms of Eqs. (1) and (2) as a function of the rod-to-grain size ratio D/d. Same data symbols as in Fig. 4 with different colors for different grain sizes: $d = 0.3$ mm (green), 1 mm (black), 2 mm (blue), and 5 mm (red).

to decrease from about 10 to 1 when D/d increases from 1 to 10. Considering a typical value $K\mu \simeq 0.2$ would lead to C_2 values from about 50 down to 5, corresponding to a range similar to C_1.

Let us now look at the question of the buckling or nonbuckling for the thin rod penetrating into grains. Considering
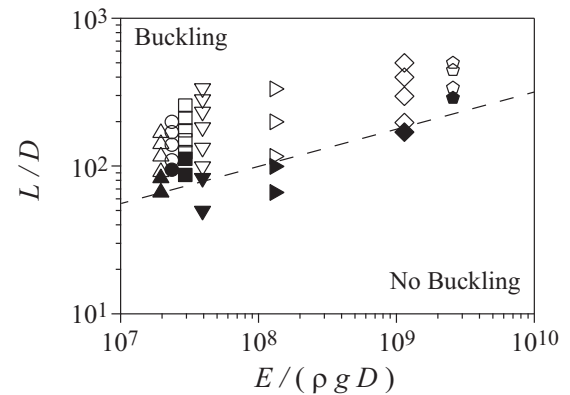

FIG. 6. Experimental observation of buckling (open symbols) or nonbuckling (filled symbols) in the parameter space given by the rod size aspect ratio L/D and the rod-to-grain stress ratio $E/\rho gD$ for all the experiments in $d = 1$ mm grains [same data symbols as in Fig. 4(a)]. (- - -) $L/D = \alpha(E/\rho gD)^{1/4}$ inferred from the modeling Eqs. (1)–(3) with $z_c = L$ and $\alpha = 1$.

that buckling should occur up to the maximal possible rod penetration $z_c = L$ leads to the buckling condition $L/D \gtrsim \alpha(E/\rho g D)^{1/4}$ with $\alpha = (\pi^2/32\varepsilon^2\phi C_2 K\mu)^{1/4}$, as the quadratic term of Eq. (2) dominates at large penetration depth ($z_c/D \gg 1$ as $L/D \gg 1$). This simple modeling predicts thus that for a rod of a given aspect ratio L/D, buckling or not buckling is governed by the rod-to-grain stress ratio $E/\rho g D$ that corresponds to the balance of the elastic modulus of the rod to the typical pressure scale of the grains at the penetration depth D. Figure 6 gathers all the data points where buckling is observed (open symbols) or not (filled symbols) in the parameter space ($L/D, E/\rho g D$). As there is some dispersion in the $C_2 K\mu$ values, α varies accordingly in the typical range $0.6 < \alpha < 1.2$ for $10 > C_2 K\mu > 1$. The theoretical line $L/D = \alpha(E/\rho g D)^{1/4}$ shown in Fig. 6 gives a rather good prediction for the buckling-nonbuckling transition when considering the dispersion of α values.

V. CONCLUSION

In this paper, we focus on the possible buckling of a thin rod when vertically plunged into a granular medium. A simple modeling with two vertical force terms, a linear one and a quadratic one for the depth dependence, allows one to recover most of the experimental observations for the buckling to appear. As long as the intruder is sufficiently immersed in the granular material, the granular material acts as an embrace leading to an effective fixed boundary condition for the bottom end of the rod. In such conditions, the critical buckling depth exhibits two scaling laws depending on the force term that prevails with a crossover between the two regimes. In the modeling developed in the present paper, the granular "radial stress" σ_{rr} is not taken into account. Recent experiments on the buckling of a thin lamella partially immersed in granular matter clearly shows that this confinement may be important [23] and elastogranular interactions have been shown recently to display intricate coupling [26]. A more refined model taking into account this granular radial stress will certainly be interesting to develop.

[1] B. Andreotti, Y. Forterre, and O. Pouliquen, *Granular Media: Between Fluid and Solid* (Cambridge University Press, Cambridge, UK, 2013).

[2] H. J. Melosh, *Research Supported by NASA*, Oxford Monographs on Geology and Geophysics No. 11 (Oxford University Press, New York, 1989), p. 253.

[3] R. D. Maladen, Y. Ding, C. Li, and D. I. Goldman, Science **325**, 314 (2009).

[4] O. Zik, J. Stavans, and Y. Rabin, Europhys. Lett. **17**, 315 (1992).

[5] G. A. Caballero-Robledo and E. Clément, Eur. Phys. J. E **30**, 395 (2009).

[6] R. Albert, M. A. Pfeifer, A.-L. Barabási, and P. Schiffer, Phys. Rev. Lett. **82**, 205 (1999).

[7] R. Candelier and O. Dauchot, Phys. Rev. Lett. **103**, 128001 (2009).

[8] A. Seguin, Y. Bertho, P. Gondret, and J. Crassous, Europhys. Lett. **88**, 44002 (2009).

[9] A. Seguin, Y. Bertho, P. Gondret, and J. Crassous, Phys. Rev. Lett. **107**, 048001 (2011).

[10] A. Seguin, Y. Bertho, F. Martinez, J. Crassous, and P. Gondret, Phys. Rev. E **87**, 012201 (2013).

[11] F. Guillard, Y. Forterre, and O. Pouliquen, Phys. Rev. Lett. **110**, 138303 (2013).

[12] A. Seguin, C. Coulais, F. Martinez, Y. Bertho, and P. Gondret, Phys. Rev. E **93**, 012904 (2016).

[13] M. B. Stone, R. Barry, D. P. Bernstein, M. D. Pelc, Y. K. Tsui, and P. Schiffer, Phys. Rev. E **70**, 041301 (2004).

[14] I. Albert, J. G. Sample, A. J. Morss, S. Rajagopalan, A.-L. Barabási, and P. Schiffer, Phys. Rev. E **64**, 061303 (2001).

[15] Y. Ding, N. Gravish, and D. I. Goldman, Phys. Rev. Lett. **106**, 028001 (2011).

[16] A. Seguin and P. Gondret, Phys. Rev. E **96**, 032905 (2017).

[17] Z. Peng, X. Xu, K. Lu, and M. Hou, Phys. Rev. E **80**, 021301 (2009).

[18] E. Hamm, F. Tapia, and F. Melo, Phys. Rev. E **84**, 041304 (2011).

[19] F. Tapia, D. Espíndola, E. Hamm, and F. Melo, Phys. Rev. E **87**, 014201 (2013).

[20] E. Kolb, C. Hartmann, and P. Genet, Plant Soil **360**, 19 (2012).

[21] N. Algarra, P. G. Karagiannopoulos, A. Lazarus, D. Vandembroucq, and E. Kolb, Phys. Rev. E **97**, 022901 (2018).

[22] M. Fakih, J.-Y. Delenne, F. Radjai, and T. Fourcaud, EPJ Web Conf. **140**, 14013 (2017).

[23] A. R. Mojdehi, B. Tavakol, W. Royston, D. A. Dillard, and D. P. Holmes, Extreme Mech. Lett. **9**, 237 (2016).

[24] A. Seguin, Y. Bertho, and P. Gondret, Phys. Rev. E **78**, 010301 (2008).

[25] W. Kang, Y. Feng, C. Liu, and R. Blumenfeld, Nat. Commun. **9**, 1101 (2018).

[26] D. J. Schunter, M. Brandenbourger, S. Perriseau, and D. P. Holmes, Phys. Rev. Lett. **120**, 078002 (2018).